Physical modeling II : directivity patterns of disc transducers

Joe Wong and Faranak Mahmoudian

ABSTRACT

In seismic physical modeling, piezoelectric transducers are commonly used as generators and detectors of acoustic waves. Physically, these transducers are thin discs with diameters on the order of 1 to 13 mm. In a typical scale model experiment where the acoustic medium is water, dominant frequencies are on the order of 500 kHz, and wavelengths are on the order of 3 mm. Even the smallest transducers have diameters which are significant fractions of a wavelength. Because of this, the radiation and reception patterns of such transducers have pronounced directivities due to wave interference effects. Amplitude information acquired by physical modeling must be corrected to account for the directivities before doing any AVO/AVAZ analysis. This report presents a numerical procedure for determining the directivities of disc-shaped transducers in an acoustic medium such as water. As well, a compact analytical formula for the directivity is derived. We applied these directivity corrections to the reflected amplitudes from a scale model experiment to illustrate their use in AVO analysis.

INTRODUCTION

The University of Calgary Seismic Physical Modeling System can be used to acquire seismograms on physical models that are scaled-down versions of idealized geological targets. Dimensions are scaled so that 1 mm in the physical model represents 10 m in the real world, and frequencies are scaled so that 1 MHz in the physical model represents 100 Hz in the real world. Piezoelectric transducers are used as generators and detectors of acoustic and/or elastic waves.

These transducers are in the shape of thin discs with diameters on the order of 1 to 13 mm. Since they operate at dominant frequencies of 0.2 to 1.0 MHz in media with velocities of 1500 to 6000 m/s, the diameters are significant fractions of a wavelength. For example, transducers with diameters of 2.4 mm, operating in water and generating signals with dominant frequencies near 500 kHz, have a diameter-to-wavelength ratio of about 0.75. They do not radiate as point sources, or receive as point detectors. In the far field, the radiation and reception patterns of such transducers have pronounced directivities caused by wave interference effects. When investigating AVO or AVAZ using data acquired with such transducers, corrections to the measured signal amplitudes must be made to account for the directivities before AVO/AVAZ analysis using standard techniques can be done.

This report presents a numerical procedure as well as a compact analytical formula for determining the directivities of disc-shaped transducers in an acoustic medium. Calculated directivities are applied to the reflection amplitudes of physically-modeled seismograms acquired over a flat water-solid interface. The corrected amplitudes are then compared to predictions from standard AVO formulas that assume no angular dependence in either the radiated field or the reception sensitivity.

CALCULATION OF THE DIRECTIVITY OF A DISC TRANSDUCER

Figure 1(a) is a schematic of a disc transducer radiating into an acoustic medium. The large semi-circle identifies the receiver point positions. They are all at the same distance R from the center of the disc but at different angles θ relative to the axis of the disc. The distance R is much larger than the radius a of the disc.
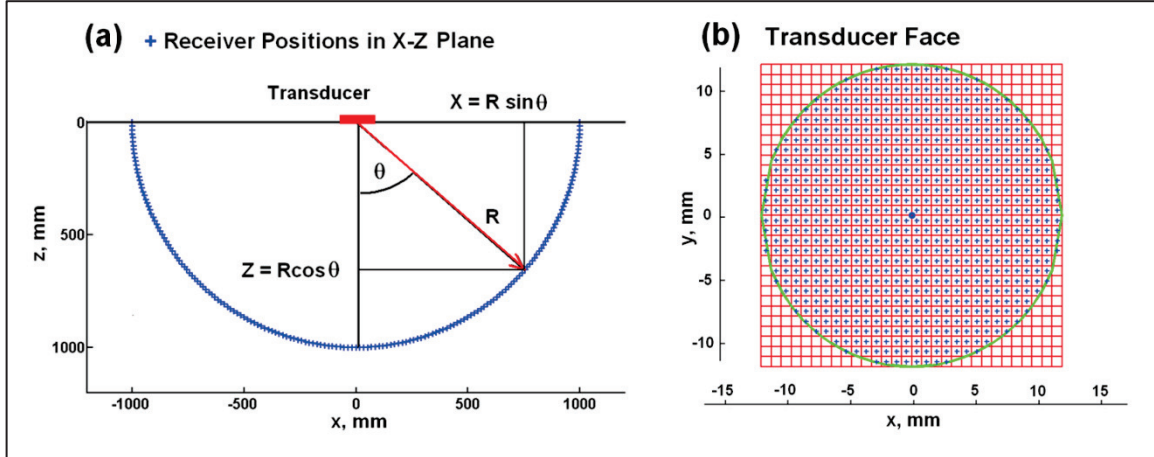

FIG. 1. (a) Geometry for calculating the radiation directivity of a disc transducer. (b) Transducer face divided up into many small surface elements inside the green circle. Typically, the diameter D of the disc transducer is in the range 1 mm to 13 mm.

Numerical calculation

On Figure 1(b), we have shown the face of a thin disc transducer with diameter D. The face is divided up into many small square elements. Each of the elements within the circumference of the disc acts as an independent source radiating isotropicly into the acoustic medium, producing a pressure field of the form

$$u = \text{real}\{\exp(-ikR)/R\} \ , \tag{1}$$

$$k = 2\pi f/c = 2\pi/\lambda \ , \tag{1a}$$

where k is the wavenumber. The frequency f typically is in the range 50 kHz to 1000 kHz. The velocity c for water is 1485 m/s, so the wavelength λ is in the range 1.5 mm to 30 mm.

The total field is the sum of fields from all the individual source elements s, and is given by

$$U_r = \sum_s \cos(k|r_r - r_s|)/|r_r - r_s|(\Delta x_s \Delta y_s) \ , \tag{2}$$

$$|r_r - r_s| = \sqrt{(x_r - x_s)^2 + (y_r - y_s)^2 + (z_r - z_s)^2} \ , \tag{2a}$$

where (x_r, y_r, z_r) are the coordinates of the observation points, and (x_s, y_s, z_s) are the coordinates of the source elements on the face of the disc located at $z_s = 0$.

Since the geometry is symmetric about the axis of the disc, we can restrict the observation points to the plane $y_r = 0$ without loss of generality. The observation

point coordinates are ($R\sin\theta$, 0, $R\cos\theta$), where θ is the angle measured from the axis of the disc. In the numerical evaluation of Equation 2, R is set to 1000 mm so that we are in far-field conditions with the distance R much greater than the wavelength λ and the disc diameter D. Keeping R constant while θ is allowed to vary, and normalizing the absolute value of U_r, we obtain the amplitude variation as a function of angle, i.e., the directivity, of the disc radiator. The summation in Equation 2 is easily done in MATLAB code.

Analytical expression

The numerical procedure for finding directivity is straightforward and flexible, and can be modified to accommodate any shape of radiating transducer. For the particular shape of a thin disc of radius $a = D/2$, we can derive a closed-form analytical expression for the directivity.
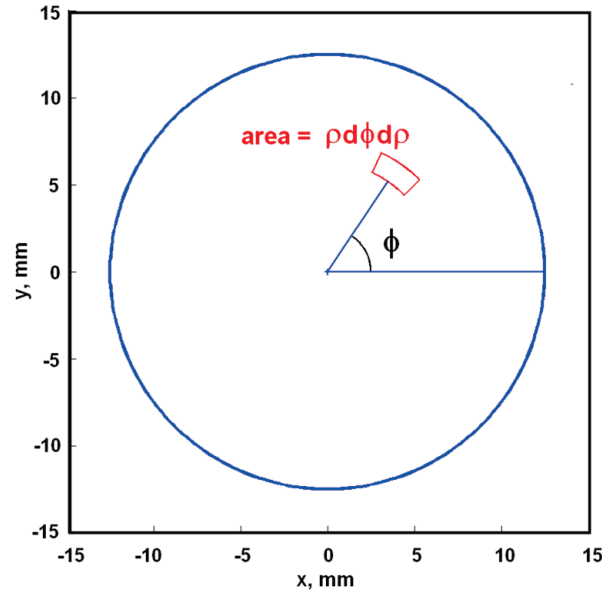

FIG. 2. The face of the disc transducer in cylindrical coordinates. The small surface element outlined in red has area $\rho d\phi d\rho$.

Figure 2 shows the face of the disc with a small surface area defined in cylindrical coordinates. The field due to many small surface elements is the integral over the entire face of the disc. Thus, the equivalent of the summation in Equation 2, expressed in cylindrical coordinates, is

$$U_r = \int_0^a \left[\int_0^{2\pi} (\cos (k|r_r - r_s|)/|r_r - r_s|)\rho d\phi \right] d\rho \ , \tag{3}$$

$$|r_r - r_s| = \sqrt{(x_r - x_s)^2 + (y_r - y_s)^2 + (z_r - z_s)^2} \ , \tag{4}$$

$$x_s = \rho \cos \phi, \ y_s = \rho \sin \phi, \ z_s = 0 \ , \tag{4a}$$

$$x_r = R\sin(\theta), \ y_r = 0, \ z_r = R\cos(\theta) \ . \tag{4b}$$

where $a = D/2$ is the radius of the disc. Substituting the quantities of Equations 4a and 4b into Equation 4, we have

$$|r_r - r_s| = \sqrt{(x_r - \rho \cos \phi)^2 + (\rho \sin \phi)^2 + (z_r - z_s)^2} \ ,$$

$$|r_r - r_s| = \sqrt{x_r{}^2 + z_r{}^2 + \rho^2 - 2x_r\rho \cos(\emptyset)} \ ,$$

$$|r_r - r_s| = \sqrt{R^2 + \rho^2 - 2R \sin \theta \, \rho \cos(\emptyset)} \ . \tag{5}$$

When $R \gg \rho$, $(R^2 + \rho^2) \sim R$, we get

$$|r_r - r_s| \sim R\sqrt{1 - 2 (\sin \theta /R) \, \rho \cos(\emptyset)} \ ,$$

$$|r_r - r_s| \sim R \left[1 - (\sin \theta /R) \rho \cos(\emptyset) \right] = R - (\rho \sin \theta) \cos \phi \ . \tag{6}$$

We use Equation 6 in Equation 3 which becomes

$$U_r \sim \int_0^a \left[\int_0^{2\pi} \{ \cos (kR - k\rho \sin \theta \cos \phi \} / (R - \rho \sin \theta \cos \phi) \rho d\phi \right] d\rho \ . \tag{7}$$

Since $R \gg \rho$, the denominator simplifies to R, and we have

$$1/R \int_0^a \left[\int_0^{2\pi} \{ \cos(kR) \cos(k\rho \sin \theta \cos \phi) + \sin(kR) \sin(k\rho \sin \theta \cos \phi) \} d\phi \right] \rho d\rho \ .$$

The integral $\int_0^{2\pi} \sin(k\rho \sin \theta \cos \phi) \, d\phi$ is zero, so we are left with

$$U_r \sim (\cos(kR) /R) \int_0^a \left[\int_0^{2\pi} \{ \cos(k\rho \sin \theta \cos \phi) \} d\phi \right] \rho d\rho \ . \tag{8}$$

From Abramowitz and Stegun (1972, Equation 9.1.2), the remaining integral over the angle ϕ is the Bessel function $2\pi J_0(\beta\rho)$, $\beta = k \sin \theta = 2\pi(\sin \theta /\lambda)$, and so

$$U_r \sim (2\pi \cos(kR) /R) \int_0^a J_0(\beta\rho) \rho d\rho \ . \tag{9}$$

From Gradshteyn and Ryzhik (1965, Equation 5, Section 6.561), we have

$$\int_0^1 x J_0(sx) dx = J_1(s)/s \ . \tag{10}$$

From Abramowitz and Stegun (1972, Equation 11.3.20), we have

$$\int_0^a t J_0(t) dt = a J_1(a) \ . \tag{11}$$

Either expression can be used to evaluate the integral in Equation 9. We will put Equation 9 into the form of Equation 11 by making the substitution $t = \beta\rho$, $t_0 = \beta a$. Then, after normalizing by $(2\pi \cos(kR) /R)$, Equation 9 becomes

$$U_r^N \sim 1/\beta^2 \int_0^{\beta a} t J_0(t) dt = (a/\beta) \cdot J_1(\beta a) \ . \tag{12}$$

We can divide U_r^N by πa^2 to get the field due to a unit source strength distributed evenly over the area of the disc:

$$U_r^N = (a/\beta) \cdot J_1(\beta a)/(\pi a^2) \, . \tag{13}$$

Substituting $a = D/2$ and $\beta = 2\pi(\sin\theta / \lambda)$ and multiplying by π, we finally have

$$U_r^N = J_1(X)/X \, , \tag{14a}$$

$$X = (\pi D \sin\theta)/\lambda \, . \tag{14b}$$

Equations 14a and 14b are identical to the expressions for directivity given by Buddensiek et al. (2009, their Equation 12) without derivation.

Directivities of vertical displacement recorded with disc transducers

A disc-shaped piezoelectric transducer is polarized in its thickness direction, so it responds to applied electric fields or strains in its thickness direction. In our physical modeling experiments, the thickness direction is the vertical direction, and the electrical output from a receiver transducer is dependent on the strain in the vertical direction on its face. The motion in an acoustic wavefield is longitudinal, i.e., the particle motion in the acoustic medium is parallel to the propagation vector. If the directivity of the total displacement field is

$$U_r^N = J_1(X)/X \, , \tag{15}$$

then the far-field reception directivity for the vertical displacement is approximately

$$u_z \sim \frac{d}{dz}(1/R) * U_r^N = (z/R) * U_r^N \, . \tag{16}$$

When a transducer is used as a source, an electric field applied across its thickness produces strain and particle motion in the vertical direction. By reciprocity, a source transducer that is identical shape to a receiver transducer has a radiation directivity also given by Equation 14. Two identical transducers used as a source-receiver pair in physical modeling measurements will have a response equal to $(u_z)^2$:

$$F(\theta) = [(z/R) * U_r^N]^2 \sim [\cos\theta * J_1(X)/X\,]^2 \, . \tag{17a}$$

Equation 17 gives the combined directivity response of a pair of identical disc-shaped transducers used to produce and detect ultrasonic acoustic waves.

Strictly speaking, the term $J_1(X)/X$ should be multiplied by the band-limited signal spectrum and integrated between its frequency limits, since the term

$$X = (\pi D \sin\theta)/\lambda = (\pi D \sin\theta) * (f/c) \tag{17b}$$

is a function of frequency. We will, however, make the simplifying assumption that result of the integration is well-approximated by the single value of $F(\theta)$ determined at the dominant frequency of the signal.

To determine directivity of the vertical component response using the numerical procedure, the summation in Equation 2 must be modified to include a factor equivalent to the $\cos\theta$ term in Equation 17:

$$v_z = \sum_s \cos{(k|r_r - r_s|)}/|r_r - r_s| * (z_r - z_s)/|r_r - r_s| * (\Delta x_s \Delta y_s)\,, \qquad (18)$$

$$z_r = R\cos\theta\,.$$

The combined directivity of identical transducers used as a source/detector pair is

$$V(\theta) = (v_z)^2\,. \qquad (19)$$

The amplitudes in a seismogram recorded with disc transducers must be corrected for the combined directivity $F(\theta)$ or $V(\theta)$ before they can be compared to standard AVO formulas that are expressed in terms of total amplitude and not vertical amplitude (Ursenbach and Hasse, 2004; Haase, 2004).

We note here that, for both the numerical summations (Equations 2 and 18) and the analytic expressions (Equations 14 and 16), the parameter that determines the wave interference effects is the dimensionless quantity D/λ.

Figure 3 plots the radiation/reception directivities due to disc transducers for three different values of D/λ. The upper curves are directivities for total displacement, while the lower curves are directivities for vertical displacement. The small circles are the numerically-determined directivities (Equations 2 and 18), while the coloured lines are values from analytic expressions (Equations 14 and 16). The numerically-determined values and the analytic values are practically identical, with small differences appearing at angles outside the range ±50º. The graphs show that as D/λ increases, the main lobe becomes narrower and more focused in the vertical direction. When D/λ exceeds 1, negative side lobes begin to form on either side of the main lobe.
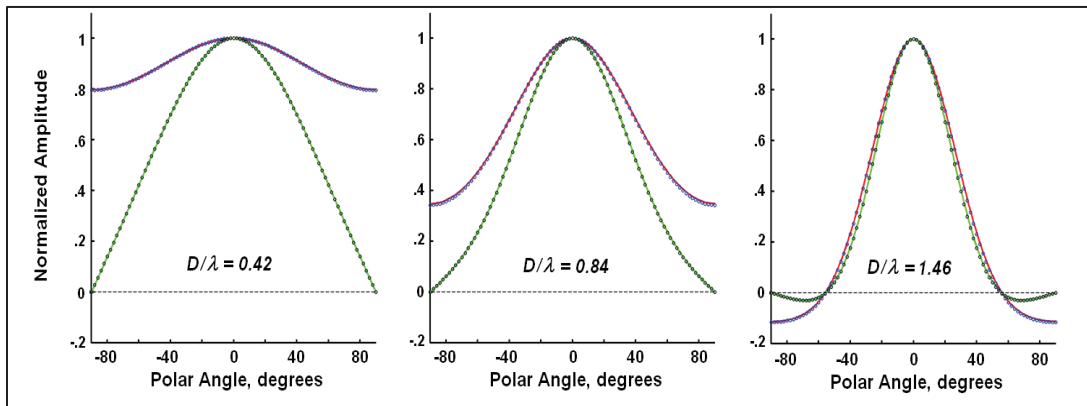

FIG. 3. Numerically-calculated directivity compared to directivity given by the analytic expression.

APPLYING DIRECTIVITY CORRECTIONS TO MEASURED DATA

Acquisition of CMP ultrasonic data

Figure 4 depicts a physical modeling survey for recording CMP (common-midpoint) gathers of seismograms over an acrylic slab (610 mm by 610 mm by 50.8 mm thick) immersed in water. The depth from the surface of the water to the top surface of the slab was about 78 mm. The gathers were along three azimuths angles (0º, 45º, and 90º) relative to the x-axis of the physical modeling system. The CMP offset increments were on the order of 5 to 8 mm, and the CMP lengths were about 300 mm. The ultrasonic

seismograms were digitized for times from 0 to 200 µs at 0.1 µs intervals. The recorded traces have dominant frequencies of about 500 kHz. Two piezopin transducers with their bottom tips slightly below the water surface were used as a source (TX) and a receiver (RX). The active piezoelectric elements in the piezopins are thin discs about 1 mm in diameter at the bottom tips. The piezopin bodies are slim brass cylinders 30.48 mm (12") long with diameters of 2.36 mm.
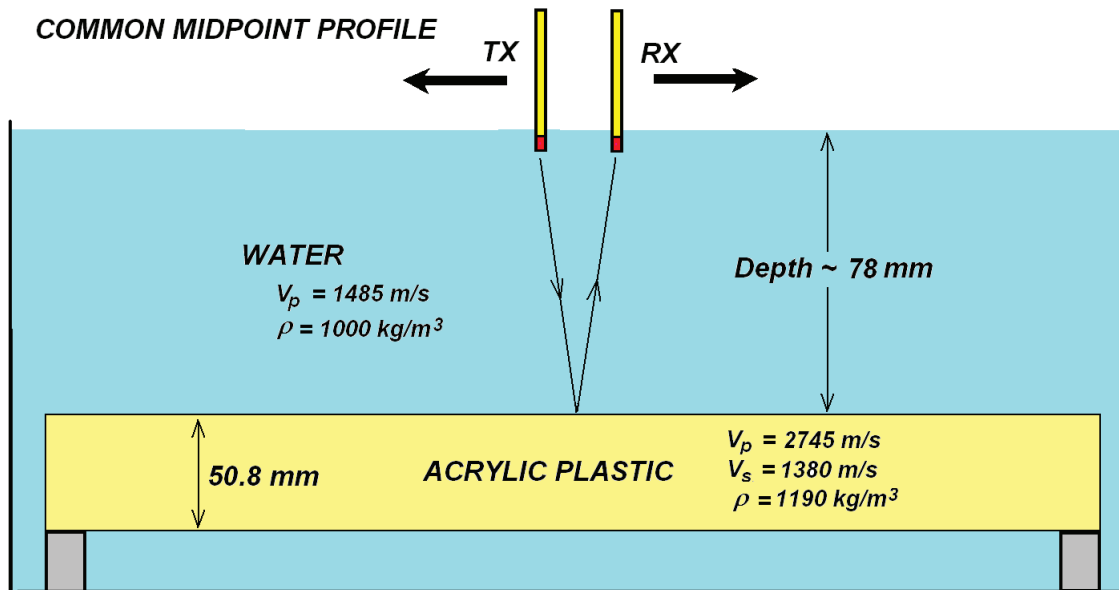

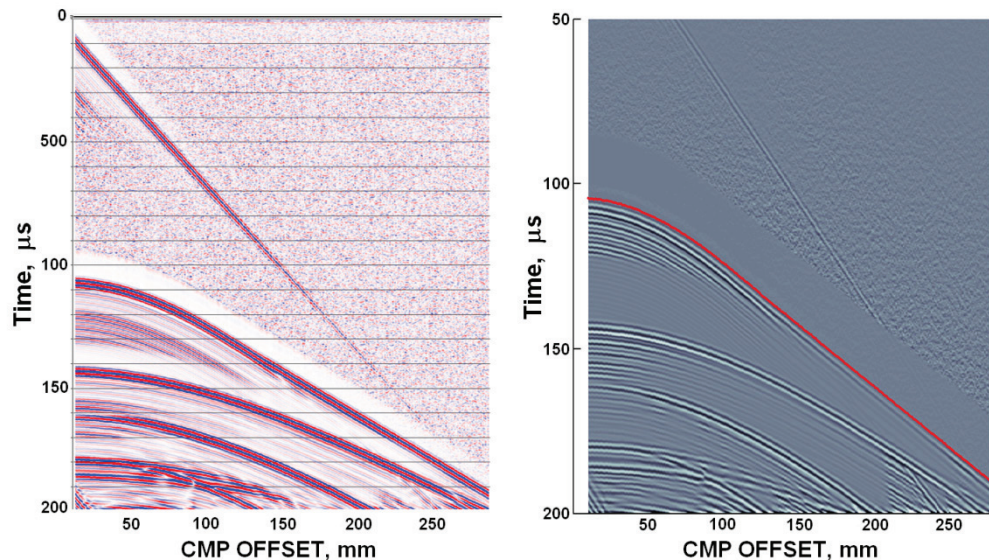FIG. 4. Acquiring ultrasonic CMP data over an acrylic slab.

FIG. 5. Left: CMP gather of ultrasonic seismograms in colour-coded AGC display. Right: gray-scale AGC display, with time picks for the reflection from the top of the acrylic plotted in red.

Figure 5 is an AGC display of the CMP gather of seismograms collected along the x-axis (azimuth = 0º). The reflection from the top water-acrylic interface begins at about 105 μs. The reflection from the bottom of the acrylic slab begins at about 140 μs.
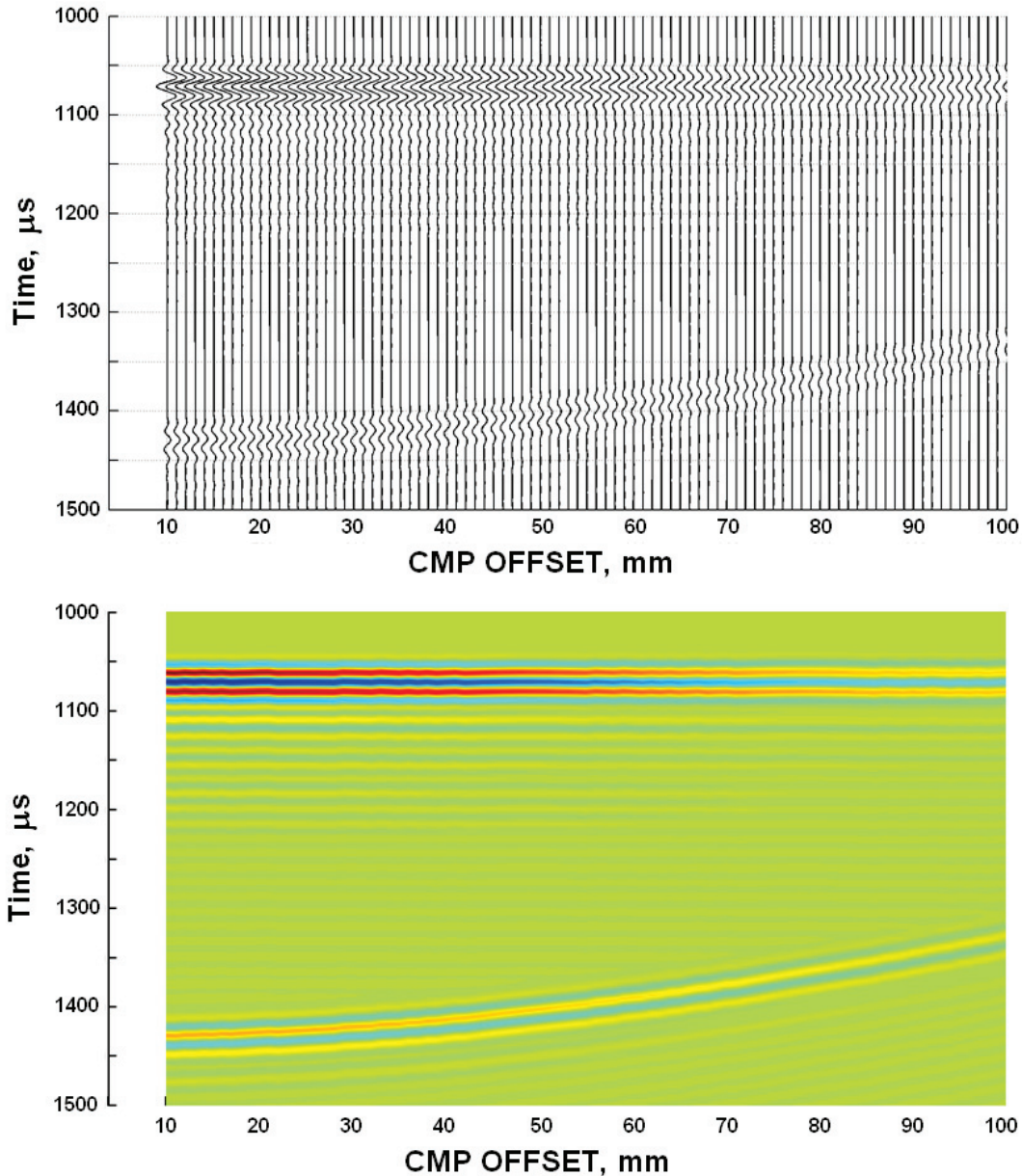

FIG. 6. Fixed-gain plots of the traces with offsets up to 100 mm, with the reflection arrivals from the top water-acrylic interface aligned according to the picked arrival times. The wiggle-trace display clearly shows the trough-to-peak amplitude variation with offset.

Figure 6 is a fixed-gain plot showing the reflection arrivals from the water-acrylic interface aligned according to the arrival times. From this figure, true relative amplitudes were estimated by picking the maximum trough-to-peak excursions of traces in 64-ms-long windows following the arrival times. Incident angles were calculated based on the

depth to the reflecting interface and the CMP offsets. The exact depth to the interface was determined by multiplying the one-way travel time on traces at the near-zero offsets by the water velocity.

Because both water and acrylic are isotropic media, the reflected signal amplitudes for all azimuths should vary with reflection angle in the same manner. On Figure 7, the amplitude-versus-angle (AVA) data for three azimuths (0º, 45º, and 90º) are plotted after being normalized by the value with angle closest to 10º. The figure shows that the amplitude variations versus incident angle for the three azimuths are practically identical, as they should be for isotropic media.
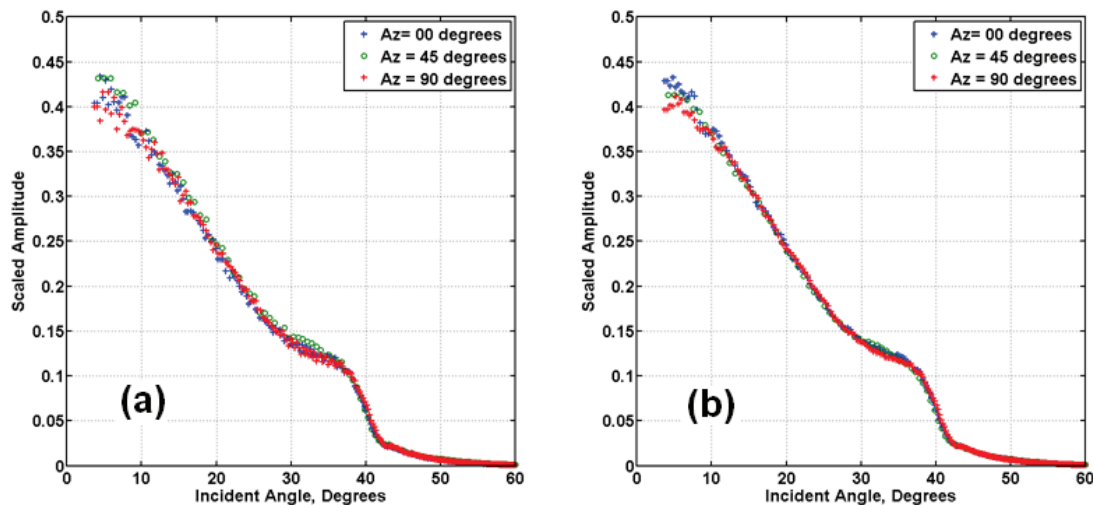

FIG. 7. AVA data for the water-acrylic reflection at three azimuth angles. (a) Raw estimated amplitudes; (b) raw amplitudes smoothed with a three-point running average.

Comparing observed reflection amplitudes with AVA predictions

The picked amplitudes on Figure 7 must be corrected for spherical divergence and the combined radiation reception directivity of Equation 17 before they can be compared to AVA predictions. The spherical divergence correction is made by multiplying the raw amplitudes by the ray lengths through water, or equivalently, by the reflection times. The directivity correction is done approximately, since the two key parameters in the equation for the combined directivity $F(\theta)$, the frequency f and the effective diameter D, must be estimated. For the frequency, we assume the dominant frequency observed on the reflected arrivals (about 520 kHz). For the diameter, we must use an effective value that is larger than the physical diameters of the disc transducers (cf. Buddensiek et al., 2010).

In our case, the increased effective diameter is mostly due to the fact that when a disc transducer is placed slightly below the surface of water, surface tension and adhesion forces between the liquid and solid surfaces causes a circular meniscus to form. The diameter of the meniscus is somewhat larger than the diameter of the transducer. On Figure 8, the menisci around two piezopin transducers whose tips are slightly below the water surface are clearly seen. The complex interaction between the piezopin tips with

the curved surfaces of the menisci force us to make best-guess estimates for the effective radiating/receiving diameters.

In making the directivity correction expressed by Equations 17a for $F(\theta)$ and 17b for $X = (\pi D \sin \theta)/\lambda$, we used $\lambda = 2.86$ mm for the wavelength in water, and $D = 4$ mm for the effective diameter.
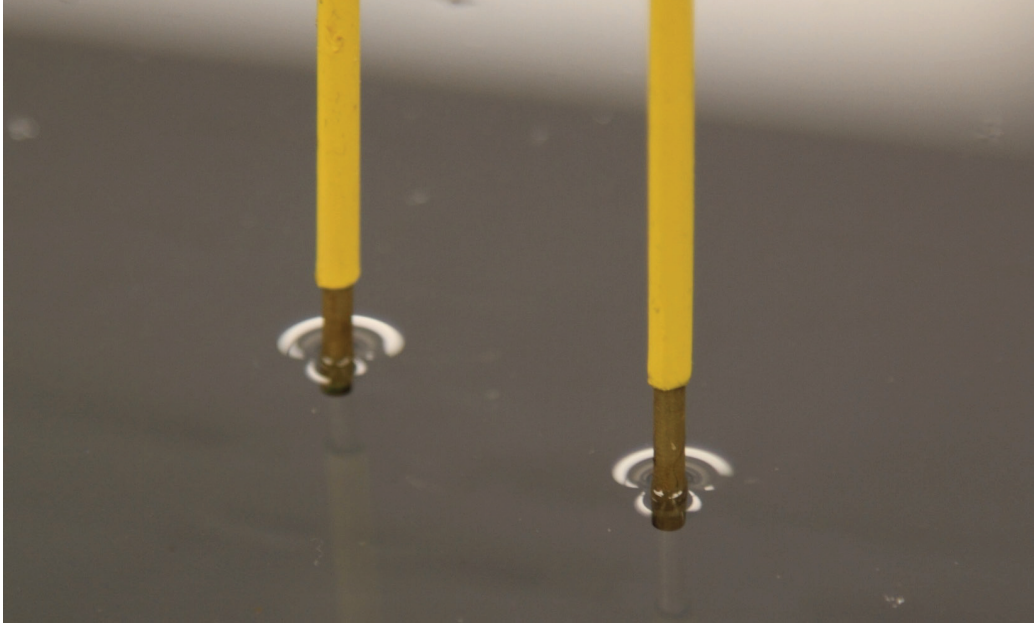

FIG. 8. Photograph of two piezopins with their tips just below the water surface. The menisci have diameters greater than the pin diameters. The diameters of the menisci are estimated to be in the range 4 mm to 8 mm, using the fact that the tip diameters of the piezopins are 2.36 mm.
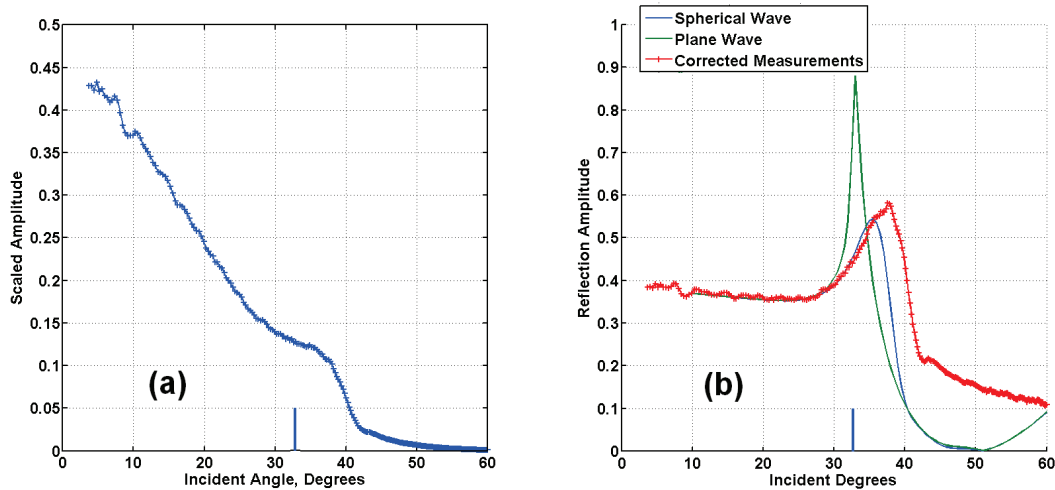

FIG. 9. (a) Raw reflection amplitudes for the water-acrylic interface; (b) directivity-corrected amplitudes (plotted in red) compared with theoretical spherical-wave and plane-wave predictions. The short blue lines on the horizontal axes mark the incident angle at 32.8º.

Figure 9 shows the results of the AVA analysis of the water-acrylic reflection on the zero-azimuth CMP profile. The raw amplitudes are shown on Figure 9a. After being corrected for spherical divergence and for the radiation/reception directivity, they are compared on Figure 9b with the theoretical AVA behavior predicted by the spherical-wave and plane-wave Zoeppritz equations ((Haase, 2004); Ursenbach and Haase, 2004). In plotting Figure 9b, the corrected amplitudes are scaled so that the corrected value at the incident angle of 10º matches the corresponding theoretical value.

For angles less than the critical angle for the water-acrylic interface (indicated by the short vertical lines at 32.8º on the horizontal axes), the AVA behaviour of the corrected amplitudes is in good agreement with both the spherical-wave and plane-wave Zoeppritz AVA predictions. For angles near critical, the spherical-wave predictions are a better fit to the observed data. For angle much beyond critical, the observed data diverges quite drastically from the theoretical values, probably because at these angles the picked amplitudes belong to the head wave arrival rather than to the reflected arrivals.

SUMMARY AND DISCUSSION

Directivities of disc-shaped piezoelectric transducers operating in an acoustic medium have been calculated numerically and analytically, and the two types of results are virtually identical. The combined radiation and reception directivities have been used to correct the reflection amplitudes measured on a physical model. The corrected amplitudes as a function of incident angle were compared to the AVA responses predicted by the plane-wave and spherical-wave Zoeppritz equations (Haase, 2004; Ursenbach and Haase, 2004). While the AVA response from the physical model conforms closely to the plane-wave Zoeppritz predictions for angle about 10 degrees less than the critical angle, it is in good agreement with the spherical-wave predictions for angles up to and slightly beyond the critical angle.

ACKNOWLEDGEMENTS

REFERENCES

Buddensiek, M.L., Krawczyk, C.M., Kukowski, N., and Oncken, O., 2009. Performance of piezoelectric transducers in terms of amplitude and waveform, Geophysics, **74**, 33-45.

Abramowitz, M., and Stegun, I.R., 1972. Handbook of mathematical functions with formulas, tables, and graphs, Dover Publications, Inc.

Gradshteyn, I.S., and Ryzhik, I.M., 1065. Tables of integrals, series, and products, Academic Press Inc.

Haase, A.B., 2004. Spherical wave AVO modeling of converted waves in isotropic media, 74th Int. Ann. Mtg, SEG Expanded Abstr. **23**, 263-266.

Ursenbach, C.P., and Hasse, A.B., 2004. An efficient method for calculating spherical-wave reflection coefficients, CREWES Research Report **16**, 60.1-60.17.

APPENDIX

The identity used in Equation 11,

$$\int x J_0(x) dx = x J_1(x) ,$$

can be established by examining the series expansions of the Bessel functions $J_0(x)$ and $J_1(x)$. Abramowitz and Stegun (1972, Equation 9.1.2)), gives the k-th term in the series expansion of $J_0(x)$:

$$(-\frac{1}{4}x^2)^k * (\frac{1}{(k!k!}) , \quad k = 0, 1, 3, \ldots$$

Multiplying by x and integrating, this term becomes

$$(-\frac{1}{4})^k x^{2k+2} * \left(\frac{1}{(k!k!(2k+2))}\right) = x(x/2)(-\frac{1}{4}x^2)^k * (\frac{1}{(k!(k+1)!}) ,$$

which is the k-th term of $x J_1(x)$.

For example, the 0-th term of $J_0(x)$ is 1. Multiplying by x and integrating, we get $x^2/2$, the 0-th term of $J_1(x)$.